ORIGINAL ARTICLE

Role of Bone Marrow-Derived Mononuclear Stem Cells versus *Nigella Sativa* Oil on Jejunal Alterations in Diabetic Adult Male Albino Rats

Samar M. Abd El-Moneam[1], Hoda H. Hussein[1], Magdy M. Omar El-Fark[1], Mona H. Mohammed Ali[1], Eman Mohammed Kamel[1]*

[1] Department of Human Anatomy & Embryology, Faculty of Medicine, Suez Canal University, Ismailia, Egypt

*Corresponding Author:

Eman Mohammed Kamel

Department of Human Anatomy & Embryology, Faculty of Medicine, Suez Canal University, Ismailia, Egypt.

E-mail:

Eman.M.Kamel@med.suez.edu.eg

ABSTRACT

Background: Several studies have revealed that *Nigella sativa* (NS) has anti-diabetic potential. Moreover, bone marrow-derived mononuclear cells (BMMNCs) have already been employed effectively as a form of regenerative therapy in different organs and tissue disorders. The aim of the work is to study the effect of BMMNCs versus *NS* oil on jejunal alterations in diabetic rats.

Methods: Forty-nine adult male albino rats were divided into rats divided into Control (I, II, III), diabetic, diabetic+BMMNCs, diabetic+Nigella sativa oil (NSO), and diabetic+insulin groups. All the tested animals were put under anaesthesia and sacrificed at the end of the experiment. Ten centimetres segment of jejunum was obtained, and half of the length of each specimen was prepared for light microscopic assessment. The other half was prepared for scanning electron microscopic examination. The findings were recorded, and statistically assessed.

Results: Diabetic plus BMMNCs group showed partial improvement in restoring almost the regular appearance of the mucosa, where most of the villi were hypertrophied with epithelium shedding. The myenteric plexus revealed a mildly increased count of nerve cells, enteric glial cells, and unmyelinated nerve fibres. The Diabetic plus NSO-treated group showed slight improvement in architecture of the villi. The Diabetic plus an insulin-treated group restored the jejunum normal architecture with different layers' normal thickness. The myenteric plexus restored its nerve cells, enteric glial cells, and nerve fibres.

Conclusions: Nigella sativa oil induces more improvement in diabetes-induced intestinal derangement as evidenced histologically and morphometrically following the diabetic plus insulin, while BMMNCs showed the least intestinal improvement in the diabetic rats.

Keywords: Nigella sativa; Insulin; Stem cells; Diabetes

INTRODUCTION

Diabetic gastrointestinal disorders (DGID) are a common complication because diabetes mellitus (DM) can affect the entire gastrointestinal tract (GIT) and cause disorders due to several factors [1], including hyperglycaemia, abnormal autonomic neuropathy, smooth muscle damage, and decreased motility in various GIT regions[2,3].

Previous studies have linked diabetes-related problems to intestinal wall hyperplasia, an increase in the small intestine's overall surface area [4], intestinal mucosa hypertrophy [1], and an increase in goblet cells [5].

Chronic hyperglycaemia depletes the antioxidative defence system activity, increases free radicals production, and induces high oxidative stress [6]. Oxidative stress causes damage to GIT cells while also impairing the endogenous antioxidant defence system [7].

Treatment for insulin-dependent diabetes mellitus typically involves insulin therapy (IDDM). However, it does not induce accurate control of β-cells effect on homeostasis of blood glucose level. It does not prevent the development of complications [8]. IDDM has no preventive measures, and the sole goal of treatment is to postpone the onset of diabetic complications [9].

Hypoglycaemia, weight gain, insulin allergy, and lipohypertrophy at insulin injection sites are the most and severe side effects of insulin therapy [10]. Moreover, the recent discovery of insulin resistance in type 1 diabetes patients has focused attention on other new relatively non-toxic therapeutic agents required to treat hyperglycaemia [11].

Nigella sativa (NS) is a spice plant in the Ranunculaceae family that is also known as habbat el Baraka or habbahsaouda" [12]. Nigella sativa's hypolipidemic [13] radical scavenging [14] and hypoglycemic properties are well known [15]. Furthermore, several studies have reported that NS has anti-diabetic properties by stimulating insulin secretion, reducing deterioration of pancreatic-cell function through antioxidative properties, and decreasing liver gluconeogenesis [16,17 18,19].

The physiological control of blood glucose levels can be achieved effectively by replacing the β-cell mass [20], which can be restored by using stem cell therapy. Stem cells are primitive, multipotent cells found in multicellular organisms. Bone marrow-derived mono-nuclear cells (BM-MNCs) represent a heterogeneous population including a mixture of a diverse array of cells; endothelial progenitor cells, multipotent adult progenitor cells and a few hematopoietic and mesenchymal stem cells [21,22]. Furthermore, BM-MNCs have been successfully used as regenerative therapy in various organs and tissues, including the heart, kidney, liver, peripheral nervous system, and tendons [23]. Furthermore, bone marrow stem cells (BMSC), hematopoietic stem cells, and endothelial cell precursors produce many cytokines and trophic factors that aid tissue recovery after injury [24]. Accordingly, current study aims to compare the effects of BM-MNCs versus NS oil and insulin on jejunal alterations in diabetic adult male albino rats.

METHODS

Fifty-six adult male albino rats weighing 200-250 g and aged 10-12 weeks were obtained from the animal house of the Faculty of Veterinary Medicine, Suez Canal University, and used through the current research (49 rats for experimental grouping and seven rats as bone marrow-derived mononuclear cell donors). They were kept in special wire mesh cages in a well-ventilated room and fed laboratory-pelleted food and ad libitum water consumption. Animals were kept in the Human Anatomy department's animal house at Suez Canal University, Faculty of Medicine for two weeks before the experiment to acclimate to laboratory conditions. All animal experiments comply with the ARRIVE guidelines and should be carried out in accordance with the U.K. Animals. All animal treatments were performed in conformity with the standards of the Faculty of Medicine, this study (protocol no. 3083#) was approved by ethics commission of the Faculty of Medicine, Suez Canal University.

Isolation of bone marrow-derived mononuclear cells (BM-MNCs):

Seven adult male albino rats were used as BM-MNCs donors. They were euthanised and sacrificed, and the muscles were cut to reveal and remove the femora and tibiae from both hind limbs. In a sterile container filled with Dulbecco's Modified Eagle's Medium (DMEM) (Lonza, Belgium), the obtained MNCs were put. According to **Fontes et al.** [25], BM-MNC isolation was carried out. To see the marrow cavities, the distal ends of the femora and tibiae were cut off then flushing 5 ml of DMEM through the marrow cavity and suspending it in 3 ml of phosphate-buffered saline (PBS) containing 10% foetal bovine serum (FBS), bone marrow (BM) was extracted from bones and centrifuged for 5 minutes at 160 g. The precipitated fraction was resuspended in 1 ml of PBS containing 10% FBS after removing the supernatant layer. 0.5ml of Ficoll-Paque was placed on top of this suspension. For 15 minutes, centrifugation was done at 400x g. This process produced a three-layered solution, with BM-MNCs making up the centre layer. The central layer of the BM-MNCs was removed using a pipette.

Induction of diabetes:

After an overnight fasting, the animals received an intraperitoneal injection of a single dosage of STZ (60 mg/kg body weight) dissolved in citrate buffer solution (pH 4.5) shortly before usage

[26]. This caused diabetes to be produced. Three days after the initial collection, blood samples were taken from the tail vein and examined using a glucometer. Diabetic animals were defined as having a blood glucose level of more than 250 mg/dL, and they were included in the research [27]. Throughout the investigation, measurements of blood glucose were taken twice weekly, with a fasting period of five hours required before each test up until the end of the study. The blood glucose level was evaluated by taking a blood sample from the tail vein via a small incision made in the terminal 1.5 mm of the tail and using a glucometer to examine the collected blood [28].

Experimental design:

The 49 male albino rats used in current research were randomly split into five groups with varying treatments:

(1) **Control groups (C) (21 rats):** were randomly subdivided into three subgroups (7 rats each): Group CI: animals didn't receive any treatment and served as a negative control. Group CII: animals received a single intraperitoneal injection of vehicle (citrate buffer, pH 4.5) 1 ml/kg [29] (**El Gawly et al., 2009**) and served as a positive control. Group CIII: animals received an injection of 2 ml of the saline solution via the tail vein and served as a positive control [30].

(2) **Diabetic group (DM) (7 rats):** animals received a single intraperitoneal injection (60 mg/kg body weight) of streptozotocin dissolved in citrate buffer (pH 4.7) [26].

(3) **Diabetic plus MNCs group (DM+MNCs) (7 rats):** diabetic rats received bone marrow-derived mononuclear cells (2×10^7) in sterile saline solution after 72 hours of diabetes induction via the tail vein [23].

(4) **Diabetic plus *Nigella sativa* oil group (DM+NSO) (7 rats):** diabetic rats received *Nigella sativa* oil (8 ml/Kg/day, intraperitoneally) 72 hours after induction of diabetes [28].

(5) **Diabetic plus insulin group (DM+INS) (7 rats):** diabetic rats received a daily dose of 15 IU/kg of insulin 72 hours after induction of diabetes [31].

Animals of all groups were weighed daily, and treatment doses were adjusted accordingly. At the end of the experiment, 28 days after diabetes was found, all animals were sacrificed [32].

Experimental evaluation:

At the end of the experiment, all animals were anaesthetised by intraperitoneal injection of 60 mg/kg ketamine and 5 mg/kg xylazine and sacrificed by cervical dislocation [33]. The animals were laid in supine position on the dissecting board and fixed by pins. A midline incision through skin and muscles was done from the xiphisternum to the symphysis pubis and extended laterally to achieve maximum exposure of the abdominal cavity. Fifteen cm away from the pylorus, a ten cm segment of the jejunum was obtained and rapidly cleaned from the residual contents by using a saline solution. Half of the length of each specimen (5 cm) was fixed in formalin and prepared for light microscopic assessment. The other half (5 cm) was prepared for scanning electron microscopic examination [7,32]

Histological evaluation:

I.   Light microscopic assessment

The jejunal specimens were stored in 10% formalin for one day before being processed, fixed in paraffin blocks, and sectioned. Hematoxylin and eosin (H&E) stain was used to analyse general histological features [34,35], and periodic acid schiff (PAS) stain was used to assess the carbohydrate contents of basement membranes, intestinal villous brush border, and goblet cells [34,36,37]. The findings of the sections were documented using an Olympus light microscope.

II.   Immunohistochemical assessment:

Paraffin blocks containing jejunal tissue were sectioned to a thickness of 3 µm, and then immunohistochemistry analysis was performed using Glial fibrillary acidic protein (GFAP) (mouse monoclonal antibody (1:1000 dilution); Dako Cytomation, Denmark, Produktion svej 42, 2600 Glostrup). Myenteric nerve plexuses were assessed using these GFAP immunostained slices [32].

Morphometric Analysis:

Five randomly chosen fields from ten serial sections (from each rat) were examined using the image analyser computer system utilising Image J software (NIH, Version 1.51 23 April 2018, USA).

In H&E-stained sections, the following measurements were evaluated:

A.   The height of 30 villi per animal was measured as the distance from the crypt-villous junction to its apex at a magnification of X100. Only villous profiles that included a stromal core and demonstrated continuity at their base with the inter-cryptal stroma (attached villi) were considered for inclusion [38].

B.   Crypt depth of 30 crypts per animal was measured as the distance from the crypt-villous

Volume 30, Issue 1, January 2024

junction to their tips at the lower limit of the crypts at a magnification of X100 [38]

C. The thickness of the submucosal layer at a magnification of X400 [7].

D. The thickness of the muscularis layer was measured at a magnification of X400 [7].

PAS-stained sections were also examined (at a magnification of X400) to assess the following measurements [32]:

a) The thickness of the wall of submucosal vessels at a magnification of X400.

b) The thickness of the jejunal villi's brush border membrane (BBM) at a magnification of X400.

c) The surface area of the goblet cells in the villi is shown at a magnification of X100.

GFAP immunostained slices were analysed (at a magnification of X400) to assess the nerve plexuses by estimating the area % of positively immunostained regions within the jejunal myenteric nerve plexuses [32], and the intensity of staining was divided into:

Grade 1: (no reaction).

Grade 2: (weak reaction): from 1–25%.

Grade 3: (mild reaction): from 26–50%.

Grade 4: (moderate reaction): from 51–75%.

Grade 5: (strong reaction): from 76–100%.

Scanning electron microscopic evaluation:

After being immediately preserved in a solution that contained 1.5% glutaraldehyde in phosphate buffer solution, the jejunal specimens were then post-fixed in a solution that contained 1% phosphate buffer in osmium tetra-oxide, dehydrated in acetone and dried using an apparatus that was referred to as a "critical point dryer." After that, the samples were given adequate time to air-dry thoroughly before being mounted on stubs, coated with a fragile layer of gold [40], and examined using a computer-controlled scanning electron microscope. (Model: JSM-5500 LV; JEOL, Ltd.-Japan). The SEM photographs were conducted at the Regional Center of Mycology and Biotechnology, Al-Azhar University, Cairo, Egypt.

STATISTICAL ANALYSIS

Data were analysed with IBM-SPSS statistical application ver. 17 (SPSS Inc., Chicago, IL, USA). Data was presented in terms of mean and standard deviation, differences was assessed statistically using one-way ANOVA and a significance level was less than 0.05.

RESULTS

1. Blood glucose level assessment

Throughout the study, there was no deviation in the serum blood glucose levels of the control groups (I, II, and III) from the normal range (70–110 mg/dL). All groups treated with STZ showed substantial hyperglycaemia three days after the diabetes was induced. The diabetic group displayed hyperglycaemia until the end of the experiment, with a highly significant increase in the terminal blood glucose level compared to the C (I, II, and III), DM+NSO, and DM+INS groups and a significant increase when compared to the DM+MNCs group. The random blood glucose level of the DM+INS group dropped significantly over the course of the experiment, it had reached values that were most comparable to those of the control group. Beginning on day 7, the levels of blood glucose steadily declined in the DM+NSO group, and this trend continued up until the end of the experiment. Despite this, the decline was not as great as in the DM+INS group. Compared to the diabetic group, rats in the DM+ MNCs group showed a significant gradual decrease in blood glucose levels over the course of several weeks. However, during the first two weeks following the induction of diabetes, these rats did not show any improvement in their blood glucose levels. Despite this, they continued to demonstrate highly significant hyperglycaemia throughout the duration of the experiment in comparison to the control group, the group receiving DM plus NSO, and the group receiving DM plus INS **(chart 1).**

2. Body weight assessment: -

No statistically significant difference was detected when comparing the groups' body weights at the beginning of the experiment. Regarding the amount of weight gained, all the animals that were part of the control groups (CI, CII, and CIII) displayed similar outcomes, with no discernible differences between them. Compared to the other groups, the rats with diabetes demonstrated statistically significant reduction in the weight gain they experienced. When compared to the diabetic group, the DM+INS and DM+MNCs groups showed an increase in substantial weight gain, while the diabetic group showed an extreme decline in substantial weight gain when compared to the control groups. DM+NSO showed a highly significant increase in weight gain compared to the diabetic group. It also showed a significant increase in weight gain compared to DM+MNCs, the value closest to that of the control groups. No discernible difference was detected between the other groups **(Table 1 and chart 2).**

3. Light microscopic assessment: -

(1) Control groups:

Sections of jejunum stained with haematoxylin and eosin demonstrated the same normal histological architecture in all control subgroups.

Mucosa, submucosa, musculosa, and serosa were the four layers of the jejunal wall. The mucosa was the deepest layer, consisting of villi (finger-like projections thrown into the lumen) and bordered by a single layer of tall columnar cells (enterocytes) with oval basal nuclei and acidophilic cytoplasm. The goblet cells were dispersed among the columnar cells. The bush boundary was still in place. The centre of the villi was formed by the lamina propria. Columnar epithelial cells with basal, oval nuclei bordered simple tubular invaginations at the base of the villi (intestinal glands or Lieberkuhn crypts), Panth cells, endocrine cells, and goblet cells. The submucosa comprises a layer of connective tissue that contains fibroblasts, blood vessels, and a nerve fibre plexus (Meissner's plexus). The layer of the muscularis externa was shown to have inner circular and outer longitudinal coats. A substantial nerve fibre plexus, known as the myenteric plexus, was discovered between these two muscle layers. This plexus is made up of many nerve cells, enteric glial cells, and an unmyelinated nerve fibre network (**Fig. 1**). PAS-stained sections in all control subgroups revealed jejunal villi with average intensity and thickness of positively PAS-stained brush border with goblet cells having average sized lumen filled with positively PAS-stained material (**Fig. 2**).

All control subgroups' GFAP-immune-stained sections revealed a vast myenteric plexus with a significant GFAP immune reaction, containing numerous GFAP-positive enteric glial cells surrounding many GFAP-negative nerve cells. The immunological response to GFAP was significant in enteric glial cells and associated processes (**Fig. 3**).

(2) Diabetic group:

Figures 4-6 showed the histopathological changes in H&E-stained jejunal sections in the diabetic group. They revealed villous pleomorphism, disturbed architecture of some villi with sloughing of necrotic villi into the intestinal lumen, the disappearance of the intervillous spaces, Cellular infiltration, oedema in the villi core, and regions of bleeding. Many villi hypertrophy, attaining conical shapes with loss of epithelial covering, particularly at the tip, the formation of subepithelial gaps, and a rise in the number of goblet cells. The epithelium of some villi was pulled away from the core of the underlying connective tissue in some of the twisted villi. Moreover, hypertrophied crypts, oedematous submucosa, congested submucosal blood vessels with thickened walls, areas of degenerated submucosa and increased thickness of the muscle layer with areas of disorganised muscle fibres were also seen. The myenteric plexus showed neuronal loss and vacuolation with few nerves and enteric glial cells.

PAS-stained sections in the diabetic group revealed jejunal villi with thickened, dense, intensely stained brush borders and numerous over-distended goblet cells with dense, positively PAS-stained material pouring its contents into the surface (**Fig. 7**).

GFAP immune-stained sections of the diabetic group exhibited a myenteric plexus that was tiny in size and had a poor GFAP immune-stained reaction. These sections also contained only a small number of GFAP-positive enteric glial cells and immune-negative nerve cells (**Fig. 8**).

(3) Diabetic treated with bone marrow-derived mononuclear cells:

H&E stained jejunal sections of this group showed partial improvement with structural variations compared to the control and the diabetic groups. The mucosa restored its normal appearance, and most villi were hypertrophied, showing fusion near its apex with areas of surface epithelium shedding and development of subepithelial spaces. Some crypts restored their normal shapes with a slight widening of their lumens and distortion of others. The myenteric plexus revealed a mildly increased number of nerve cells, enteric glial cells and unmyelinated nerve fibres compared to the diabetic group (**Fig. 9**).

PAS-stained sections in the DM+MNCs group showed jejunal villi with moderate intensity and thickness of PAS- positively stained villous brush border and goblet cells filled with PAS-stained material (**Fig. 10**).

GFAP immune-stained sections of the DM+MNCs showed mild GFAP immune-stained myenteric plexus, a slight increase in the number of GFAP-positively immune-stained enteric glial cells and negatively immune-stained nerve cells compared to the diabetic group but still fewer in numbers compared to the control group (**Fig. 11**).

(4) Diabetic treated with Nigella sativa oil group:

H&E stained jejunal sections of this group showed restoration of almost the normal architecture of villi compared to the control groups. However, the presence of small areas of villous loss was still obvious. Goblet cells and enterocytes looked near to those of the control groups, with the appearance of few inflammatory cells in the lamina propria. Submucosal medium-sized walled blood vessels were seen. The Muscolosa layer showed minimal fibre hypertrophy. The myenteric plexus revealed intact nerve cells, enteric glial cells and nerve fibres (**Fig. 12**).

PAS-stained sections in the DM+NSO group showed jejunal villi with mild intensity and thickness of PAS positively stained villous brush border and many appropriate-sized goblet cells filled with PAS-stained material (**Fig. 13**).

In contrast to the diabetic group, which had positive GFAP immune expression in enteric glial cells in the submucosal plexus, the DM+NSO group's myenteric plexus displayed a moderate GFAP immune-stained reaction, an increase in the number of GFAP-positive enteric glial cells, and negatively immune stained nerve cells (**Fig. 14**).

(5) Diabetic treated with insulin group:

Sections of the jejunum from this group demonstrated the return of the typical jejunal architecture, including well-formed villi and restored mucosal cellular organisation. However, few areas of epithelial sloughing were still seen. Lamina propria and crypts appeared close to the control groups, with few small goblet cells and normal-sized walls of submucosal blood vessels compared to the diabetic group. Muscular layer fibres looked like those of the control groups. The myenteric plexus restored its nerve cells, enteric glial cells and nerve fibres compared to the diabetic group (**Fig. 15**).

DM+INS group showed jejunal villi with mild intensity and thickness of PAS- positively stained villous brush borders nearly like those of the control groups. Goblet cells appeared with appropriate size filled with PAS-stained material (**Fig. 16**).

The number of GFAP-positive enteric glial cells and negatively immune-stained nerve cells was significantly higher in the DM+INS group than in the diabetic group (**Fig. 17**).

4. Morphometric results: -

I. Length of the villi: (Table 2)

In comparison to (C) groups, DM groups significantly increased villi length. Compared to the DM group, the DM+INS and DM+NSO groups displayed significantly lower villous length. DM+MNCs did not differ significantly from the DM group regarding villi length. Compared to (C) groups, DM+MNCs showed a highly significant increase in villi length, whereas DM+NSO demonstrated a significant increase. Additionally, the DM+INS group's value was the closest to that of the (C) group. When both groups were compared to the DM+MNCS group, a highly significant decrease in the villi length was reported in the DM+INS group and a substantial drop in the DM+NSO group.

II. Crypt depth: (Table 2)

Compared to the (C) groups, the crypt depth in the DM group displayed a significant rise. Compared to the DM group, all other groups demonstrated a substantial decrease in crypt depth,

except the DM+INS group, which revealed a highly significant decrease. The DM+NSO group and the DM+MNCs group also revealed a significant decline. We could not find any statistically significant differences between the other groups.

III. Submucosal thickness: (Table 2)

Submucosal thickness did not significantly differ between any of the tested groups.

IV. Musculosa thickness: (Table 2)

Compared to the (C) group, the DM group demonstrated a highly significant increase in musculosa layer thickness. In comparison to the DM group, the DM+MNCs group displayed a significantly significant reduction in musculosa layer thickness. There was no discernible difference between the other groups.

V. Thickness of submucosal vessels wall: (Table 2)

DM group showed a highly significant increase in the thickness of the submucosal vessel wall compared to (C) groups. DM+MNCs, DM+INS and DM+NSO groups showed a highly significant decrease in the thickness of the submucosal vessel wall compared to the DM group. No significant difference was observed between the other groups.

VI. Thickness of the brush border membrane (BBM) of jejunal villi*: (Table 2)

Compared to the control group, the diabetic group exhibited a highly significant increase in the thickness of the jejunal villi's brush border membrane–(BBM). When compared to the DM group, the DM+INS, DM+NSO, and DM+MNCs groups all displayed a highly significant reduction in (BBM) thickness of the jejunal villi. We could not find any statistically significant differences between the other groups.

VII. Surface area of luminal goblet cells per villus: (Table 2)

In comparison to (C) groups, the DM group demonstrated a highly significant increase in the surface area of luminal goblet cells per villus. The surface area of luminal goblet cells per villus was significantly lower in the DM+INS, DM+NSO, and DM+MNCs groups than in the DM group. There was no discernible difference between the other groups.

VIII. Percentage of GFAP-immune-stained area of myenteric plexus: (Table 2)

In comparison to (C) groups, the DM group demonstrated a highly significant decline in the proportion of the myenteric plexus that was immune-stained for GFAP. Compared to the DM group, the percentage of the myenteric plexus that was immune-stained with GFAP increased significantly in the DM+INS and DM+NSO groups. When DM+MNCs and DM+NSO were compared

to controls, the percentage of the myenteric plexus that was immune-stained with GFAP in both groups exhibited a highly significant decline. There was no discernible difference between the other groups.

5. *Scanning electron microscopic examination: -*

(1) Control groups:

Scanning electron microscopic examination of all control subgroups revealed a regular arrangement of the villi with narrow intervillous spaces. The jejunal villi appeared intact with the normal hexagonal pattern, intact surface epithelium with pockmarks corresponding to the mouth of goblet cells and scattered mucous. The microvilli were packed together with a regular appearance causing a rough surface appearance (**Fig. 18**).

(2) Diabetic group:

Scanning electron microscopic examination of the jejunum of the diabetic group revealed that most of the villi appeared distorted with necrotic tips and sloughing of the epithelial covering. The villi displayed noticeable convolutions, a rough granular look on some surfaces, and seemed wider with the loss of microvilli (Fig. 19).

(3) Diabetic treated with bone marrow-derived mononuclear cells: -

Scanning electron microscopic examination of the diabetic group treated with bone marrow-derived mononuclear cells revealed that some villi appeared with regular structure, surface and goblet cell openings. Whereas other villi still showed sloughing of their tips and loss of microvilli (**Fig. 20**).

(4) Diabetic treated with nigella sativa oil group: -

Scanning electron microscopic examination of DM+NSO revealed a nearly normal villous appearance with slight changes in the form of small areas of exfoliation of the villous epithelial lining (**Fig. 21**).

(5) Diabetic treated with insulin group: -

Scanning electron microscopic examination of the diabetic group treated with insulin revealed a similar villous structure to that of the control group. They showed a regular arrangement of the villi with intact epithelial covering cells. The jejunal villi appeared intact with a regular hexagonal pattern with a typical appearance of microvilli on the villous surface (**Fig. 22**).

Table 1: Mean ± SD of body weight and body weight gain in the studied groups

Weight \ Group	Initial body weight (gm) Mean ± SD	Terminal body weight (gm) Mean ± SD	Weight gain (gm) Mean ± SD
C I	215.4±10	261.0±23	46.1±4.9 [D, IN,ST]
CII	216.9±15.1	264.7±21.4	47.8±7.8 [D, IN,ST]
C III	216.3±13.8	260±17	43.7±7.4 [D, IN,ST]
DM	215±12	209.0±14	- 6±2.5 [C, IN, N,ST]
DM+MNCs	222±21	241.7±23	19.6±5.1 [D , C, , N]
DM+NSO	218±16.5	257.4±33.3	37.7±9 [D, ST]
DM+INS	219±14	247.0±25	28±8.2 [D ,C]

(-) loss, (+) gain

ANOVA, Post hoc test:

([C]) P<0.01 compared to the control groups.

([IN]) p<0.01   compared to insulin group

([ST]) p<0.01 compared to MNCs group

([D]) p<0.01 compared to the diabetic group

([N]) p<0.01 compared to nigella sativa group

Table 2: morphometric parameters of jejunum in all studied groups

Groups \ Parameters	Control I mean±SD	ControlII mean±SD	ControlIII mean±SD	Diabetic mean±SD	DM+ MNCs mean± SD	DM+ NSO mean± SD	DM+ INS mean± SD
Villi length (µm)	560.8 ± 61.1 [D, n, ST]	574.9± 44.6 [D, n, ST]	580.9±47.2 [D, ST]	880.8±71.9 [C, IN, N]	787.2±58.2 [C, IN, n]	678.55±52.61 [∗,D, st]	643.7± 56 [D, ST]
Crypt depth (µm)	159.26± 26.39[D]	161.64±26 [D]	163.6±29.6 [D]	278.77±88.59 [C, IN, n, St]	193.84±12[d]	202.15±14.14 [d]	186.7± 31.08[D]

Submucosal thickness (µm)	32.42 ± 11.11	31.34 ± 8.8	33.1 ± 9	46.03 ± 12.82	36.52 ± 8.7	39.31 ± 11.47	35.93 ± 4.5
Musculosa thickness (µm)	62 ± 16.05 [D]	63.1 ± 14.2 [D]	59.7 ± 9 [D]	91.86 ± 11.96 [C, ST]	66.2 ± 10.97 [D]	80.23 ± 11.35	75.12 ± 8.1
Thickness of the wall of submucosal vessels (µm)	1.89 ± 0.64 [D]	1.96 ± 0.56 [D]	2.03 ± 0.32 [D]	7.13 ± 2.4 [C, IN, N,ST]	2.94 ± 0.64 [D]	3.64 ± 1.07 [D]	3.29 ± 0.82 [D]
Thickness of BBM of jejunal villi (µm)	1.56 ± 0.62 [D]	1.49 ± 0.49 [D]	1.69 ± 4.8 [D]	6.59 ± 1.95 [C, IN, N, ST]	2.28 ± 1.08 [D]	1.99 ± 0.59 [D]	1.73 ± 0.56 [D]
Surface area of the lumina goblet cells of villous (µm^2)	5925.1 ± 1745.2 [D]	6099.2 ± 1262.8 [D]	5960.5 ± 890.7 [D]	14175.7 ± 1868.3 [C, IN, ST, N]	6409.9 ± 1176.7 [D]	6462.1 ± 2104.1 [D]	6048.3 ± 1987.4 [D]
Percentage of GFAP-immunostain area in the myenteric plexus (%)	6.29 ± 2.2 [D, n, ST]	5.95 ± 1.7 [D, st]	6.09 ± 0.7 [D, n, ST]	1.49 ± 0.78 [C, IN, N]	3.01 ± 0.79 [C]	4.07 ± 0.43 [*, D]	4.27 ± 0.69 [D]

Using ANOVA, Post hoc test

(*) p<0.05 compared to the control group.   (^{C}) p<0.01 compared to the control groups.
(^{d}) p<0.05 compared to the diabetic group.   (^{D}) p<0.01 compared to the diabetic group
(^{in}) p<0.05 compared to DM+ INS group.   (^{IN}) p<0.01 compared to DM+ INS group
(^{n}) p<0.05 compared to DM+ NSO group.   (^{N}) p<0.01 compared to DM+ NSO group
(st) p<0.05compared to the DM+MNCs group.   (ST) p<0.01 compared to DM+MNCs group
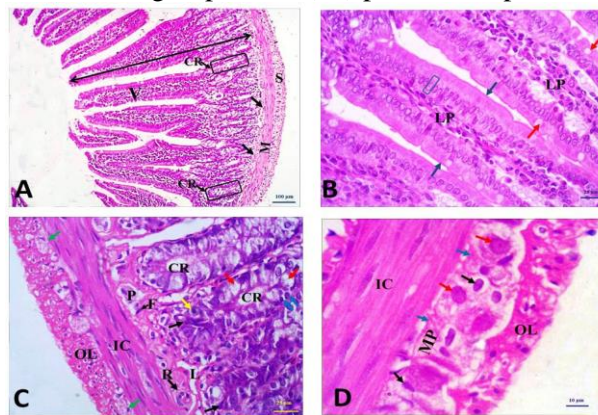
Figure 1: Photomicrographs of sections in rat jejunum of the control group showing:
(**A**) the normal architecture of the four layers of the jejunum: mucosa (double head arrow) where villi (V) appear as finger-like projections thrown into the lumen with tubular invaginations at its bases (CR), submucosa (arrows), muscularis externa (M) and serosa (S). (**H&E, X100**)
(**B**) villi appearing as finger-like projections with lamina propria (LP), covered by a single layer of tall columnar cells with oval basal nuclei (blue rectangle), goblet cells (red arrows) are scattered in-between these columnar cells. Note, intact brush border (blue arrows). (**H&E, X400**)
(**C**) crypts (CR) with lining columnar epithelium (blue arrow), paneth (black arrow), endocrine cells (yellow arrow), goblet cells (red arrows), submucosa with lymph **vessel** (L), fibroblast (F), Meissner's plexus (P), submucosal capillary with normal diameter and wall (R), inner circular (IC), outer longitudinal muscle layers (OL) and multiple myenteric plexuses (green arrows). (**H&E, X400**)
(**D**) a large well-defined myenteric plexus (MP) embedded between the inner circular (IC) and outer longitudinal muscle layers (OL). The plexus was comprised of nerve cells (red arrows), numerous enteric glial cells nuclei (black arrows), and a network of unmyelinated nerve fibers (blue arrows). (**H&E, X1000**)
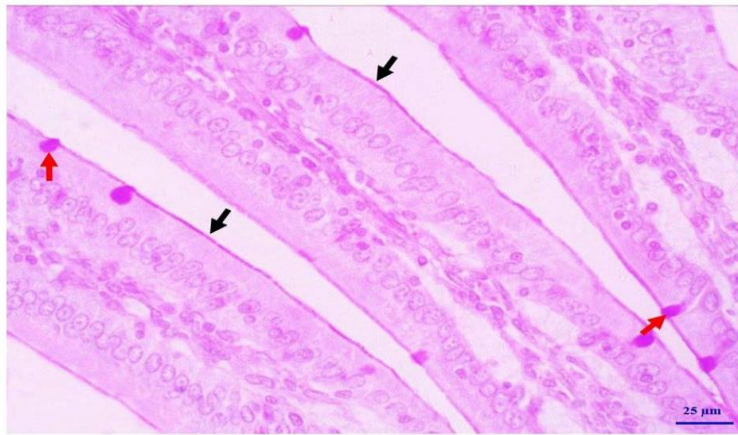
Figure 2: A photomicrograph of a section in rat jejunum of the control group showing jejunal villi with normal thickness of positively PAS-stained villous brush border (black arrow) and goblet cells with average sized lumen filled with positively PAS-stained material (red arrow). (**PAS, X400**)
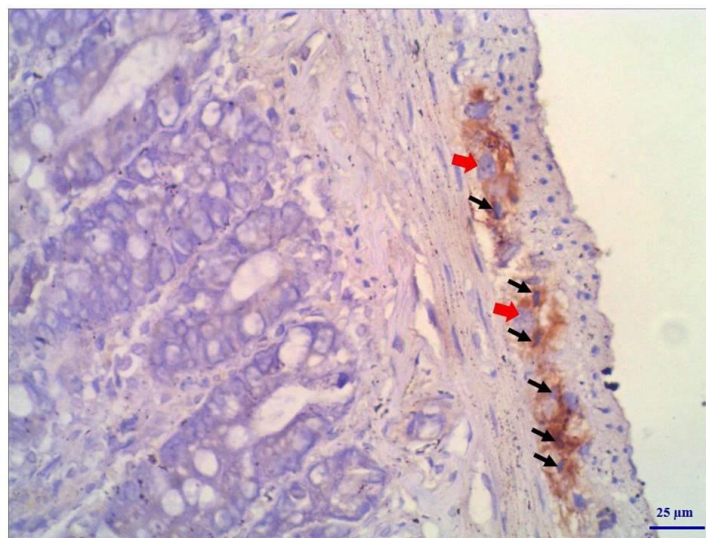

Figure 3: A photomicrograph of a section in rat jejunum of the control group showing a large well-defined myenteric plexus formed of numerous positively GFAP immune-stained enteric glial cells (black arrows) and many GFAP-negative nerve cells (red thick arrows). (**GFAP-immunostain, X 400**)
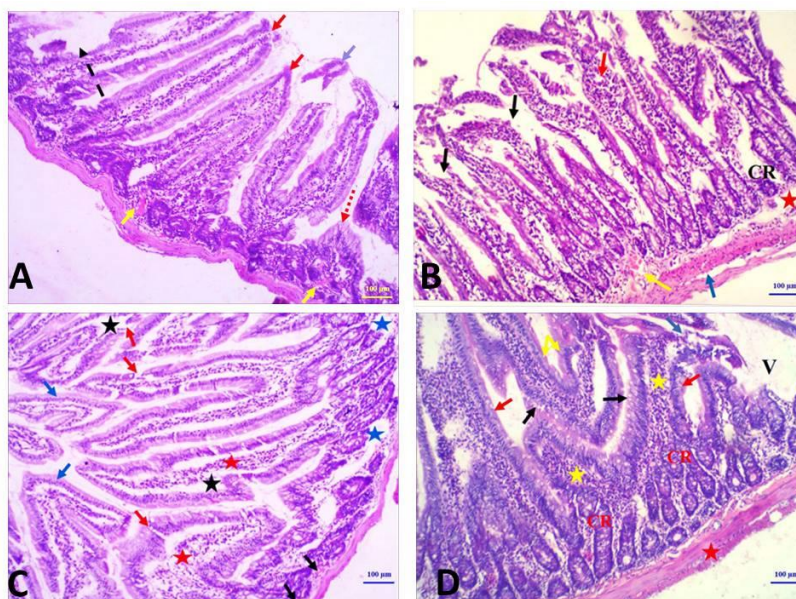
Figure 4: Photomicrographs of sections in rat jejunum of the diabetic group showing:

(A) distortion of villous architecture (black dashed arrow), sloughing of necrotic villi into intestinal lumen (blue arrow), hypertrophied villi (red thick arrows), hemorrhage (yellow arrows) and thickened broad conical shaped villi (dashed red arrow). **(H&E, X 100)**

(B) sloughing epithelial covering especially near the tips of the villi (black arrows), disappearance of the intervillous space, distortion of the crypts (CR) with extensive inflammatory infiltration (red arrow), degenerated submucosa (red star), congested submucosal blood vessel (yellow arrow) and disorganized muscle layer (blue arrow). **(H&E, X 100)**

(C) hypertrophied villous architecture with discontinuation of its epithelial lining (red arrow), heavy inflammatory infiltration (red star), presence of subepithelial spaces (black star), twisted villi showing separation of the epithelium from the underlying connective tissue core (blue arrow), vacuolation (blue star) and hemorrhage between crypts (black arrow). **(H&E, X 100)**

(D) thick hypertrophied villi (red arrows), loss of surface epithelium (blue arrow), extensive cellular infiltration (yellow star), twisted villi with separation of the epithelium from the underlying connective tissue core (yellow arrows), area of villous loss (V), hypertrophied crypts (CR), marked increase of goblet cells (black arrows) and increased thickness of muscle layer (red star). **(H&E, X 100)**
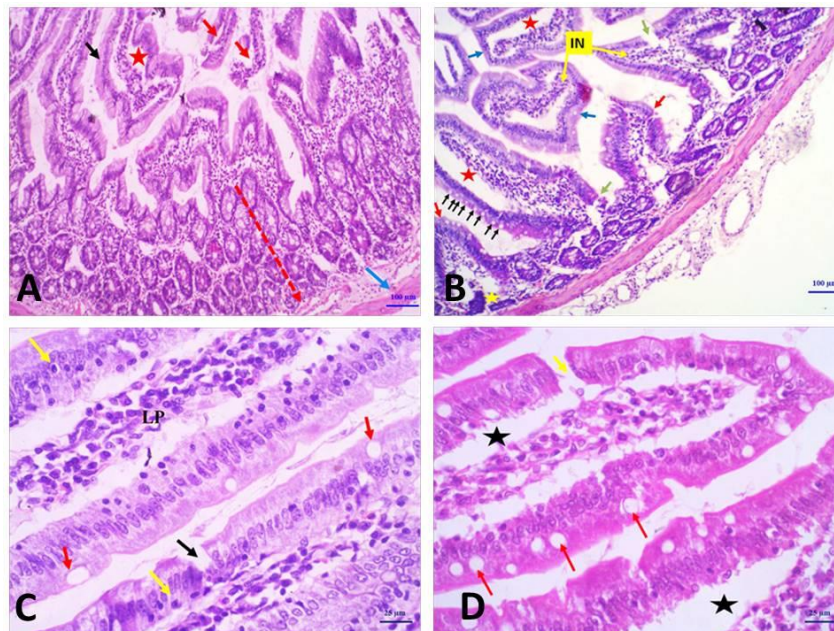
Figure 5: Photomicrographs of sections in rat jejunum of the diabetic group showing:

(A) villi losing its contact to the underlying core (black arrow) with development of subepithelial space (red star), sloughing of necrotic villi into intestinal lumen (red arrows), marked hypertrophy of crypts (dashed red arrow) and edema of submucosa (blue arrow) . **(H&E, X 100)**

(B) thick broad villi assuming conical forms (red arrows), discontinuation of the epithelial lining (green arrow), separation of the epithelium from the underlying corium with formation of wide subepithelial spaces (red stars), twisted villi (blue arrow), infiltration of lamina propria with inflammatory cells (IN), ill-defined increased number of goblet cells (black arrows) and distortion of the crypt (yellow star). **(H&E, X100)**

(C) hypertrophied villi with nuclear pyknosis of enterocytes (yellow arrow), infiltration of lamina propria (LP) with inflammatory cells, surface epithelium discontinuation (black arrow) and distended goblet cells (red arrow). **(H&E, X400)**

(D) hypertrophied villi, with areas of surface epithelium loss (yellow arrow), shrinkage and separation of the epithelium from the underlying corium with formation of wide subepithelial spaces (black star) and increased number of distended goblet cells (red arrow). **(H&E, X400)**

DISCUSSION

Diabetes mellitus affects the gastrointestinal tract, causing gastroparesis, enteropathy, and oesophageal motor dysfunction [41] and could be a predisposing factor for small intestinal bacterial overgrowth (SIBO) [42]. The goal of this study was to evaluate

the possible beneficial effects of Nigella sativa oil compared to those of bone marrow-derived mononuclear cells in reducing the harmful effects of diabetes on the jejunum of adult male albino rats.

The current study showed significant hyperglycaemia in the diabetic group, which agrees with Moezi et al. [43] who found that STZ caused pronounced hyperglycaemia four days after administration by reducing and destroying pancreatic Beta cell mass, resulting in insulin deficiency and hyperglycaemia. Moreover, the DM+MNCs group in the present study revealed a minimal significant reduction of the terminal blood glucose level compared to the diabetic group.

HbA1c levels were lower in patients with diabetes treated with MSCs, as reported by Ranjbaran et al. [44]. In addition, the DM+NSO group demonstrated a highly significant decrease in hyperglycaemia compared to the diabetic and DM+ MNCs groups, which is in line with Hamdan et al. [45]. At the end of the experiment, the DM+INS group's random blood glucose level had decreased significantly, coming close to that of the control groups. These findings agree with those found in [46,11].

The diabetic group in the present study revealed a highly significant weight loss compared to other groups, which is in accordance with [47, 48]. Al-Logmani and Zari. and Mohan et al. [13, 49] explained weight loss in diabetic as the tissues' inability to obtain their required glucose and energy, forcing the body to break down its fats and proteins for energy production, resulting in decreased muscle mass and rapid weight loss.

In the current study, the diabetic group showed jejunal histopathological alterations in the form of villous pleomorphism, disturbed villous architecture, necrosis, sloughing, the disappearance of the intervillous spaces, cellular infiltration, oedema, haemorrhage, villous hypertrophy, epithelial loss, edematous and congested submucosa, hypertrophy of muscularis layer and areas of disorganised muscle fibres. It also revealed a highly substantial lengthening of the villi, crypts, an increase in the thickness of the submucosal vessels, the thickness of the BBM of the jejunal villi, the surface area of luminal goblet cells and the thickness of the muscularis layer. Villi also revealed ultrastructure alterations in the form of distorted necrotic tips, sloughing of the epithelial covering, loss of microvilli and marked convolutions. These histological results agree with Abo Gazia and Hassan [7] (in the ileum) and Elmansy and Almasry; Eltahawy et al. [32,5] (in the jejunum). Moreover, Piccolo et al. [50] observed an increase in mucosal villi length and crypt depth in the ileum, as well as increased crypt depths in the

colon in diabetic rats. Furthermore, Lerkdumnernkit et al. [51] observed duodenal changes in the diabetic group in the form of deformed duodenal villi, disrupted surface epithelium and distorted shapes of crypts, significant increases in villus height and crypt depth, lymphoid cell accumulation in the lamina propria and decreased number of goblet cells.

As compared to the control group, the DM+MNCs group in the current study displayed partial histopathological improvement in the jejunum, a highly significant increase in villous length, a significant decrease in crypt depth, and highly significant increases in the thickness of the musculosa layer, BBM, submucosal vessel wall, and luminal goblet cell surface area. A reasonable thickness of positively stained villous brush border and less filled goblet cells with positive PAS-stained material were seen in the morphometric analysis of BBM and the luminal goblet cell surface area. The myenteric plexus was also visible in the DM+MNCs group, along with a minor increase in the proportion of enteric glial cells immunostained positively for GFAP and negatively for nerve cells. Additionally, the DM+MNCs group had a slight improvement in ultrastructure, which supported the findings from the light microscopic analysis.

These results can be explained by the occurrence of endothelial repair and inflammatory environment modulation [52], stimulation of endogenous stem cells, neovascularisation [53] and decreased oxidative stress [4]. Furthermore, [54] observed that diabetes harms the body's endogenous stem cells in every way, which can result in severe consequences. Exogenous stem cell augmentation can mitigate the effects of diabetes on the quantity and quality of stem cells. Clinical trials did not yet demonstrate safety or efficacy [55].

Additionally, the DM+NSO and DM+INS groups in the current study displayed restoration of the mucosa, lamina propria, and crypt cellular organisation, as well as villi that were practically back to their standard architecture with increased length. Additionally, they showed a considerable improvement in the DM+INS group for the crypt depth, villous length, BBM, the thickness of the submucosal vessels wall, and luminal goblet cell surface area. In contrast to the diabetic group, the DM+INS group displayed several goblet cells with the proper size and a slightly thickened villous brush border. The percentage of the myenteric plexus immunostained with GFAP increased significantly in both the DM+INS and DM+NSO groups. The number of enteric glial and nerve cells significantly increased in the DM+INS group compared to the diabetic group. Additionally, the DM+INS group's ultrastructure

results showed a picture similar to the control group, whereas the DM+NSO group's results showed a superior improvement in the intestinal ultrastructure derangement than the DM+INS group.

Previous researches explained the effect of NSO on the improvement of histopathological findings caused by diabetes by a variety of factors, including i) the anti-diabetic properties of NS [18,19], ii) the synergistic action of NSO bioactive constituents with antioxidant properties, such as thymoquinone, dithymoquinone, and carvacrol, in neutralising diabetes-generated free radicals and antagonising the enhanced oxidation of membrane lipids and proteins, thereby preserving the functional and structural integrity of the brush border membrane (BBM) [14, 56], iii) the polyunsaturated fatty acids of NSO may substitute the polyunsaturated fatty acid components of BBM that had been oxidatively damaged by ROS, thereby, accelerating the repairing process and restoring membrane integrity [57].

Moreover, Hannan et al. [58] concluded that Nigella sativa seeds extract has anti-hyperglycaemic activities either normoglycemic or diabetic animals by decreasing intestinal glucose absorption, increasing tissue glucose utilisation, and improving insulin release. Furthermore, Alireza et al. [59] found that NSO supplementation in diabetic haemodialysis patients reduced oxidative stress and inflammatory markers however HbA1c and fasting blood sugar levels were still elevated.

On the other hand, Charlton et al., [60] attributed the intestinal improvement in diabetic rats treated with insulin to maintain the normal rates of protein synthesis in the in the mucosa of the small intestine, which is an essential component of the remodelling process of this fast turning over the tissue. The decline in the rate of protein synthesis in the mucosa of small intestinal during insulin deprivation may play a role in the development of gastrointestinal complications in poorly controlled type 1 diabetic patient.

CONCLUSIONS

This study showed that NSO induced better improvement in diabetes-induced intestinal derangement following diabetic plus insulin, while MNCs caused the least intestinal improvement in diabetic rats. Therefore, Patients with diabetes may be offered NSO supplementation to lessen the damaging effects of diabetes mellitus on the digestive tract.

RECOMMENDATIONS

Nigella sativa oil supplementation could be prescribed for diabetic patients in order to improve the intestinal abnormalities. Further studies should be carried out to investigate the possible protective effect of prolonged use of bone marrow derived mononuclear cells on diabetes.

REFERENCES

1. **Zhao, M., Liao, D., & Zhao, J.** Diabetes-induced mechanophysiological changes in the small intestine and colon. WJD 2017**;**8(6), 249-69.

2. **Durmus-Altun, G., Vatansever, U., Vardar, S. A., Altaner, S., & Dirlik, B.** Scintigraphic evaluation of small intestinal transit in the streptozotocin induced diabetic rats. Hippokratia 2011;15(3), 262 –4.

3. **Liu, W., Yue, W., & Wu, R.** Effects of diabetes on expression of glial fibrillary acidic protein and neurotrophins in rat colon. Auton Neurosci 2010;154(1-2), 79-83.

4. **Chen, P., Zhao, J., & Gregersen, H.** Up-regulated expression of advanced glycation end-products and their receptor in the small intestine and colon of diabetic rats. Dig Dis Sci 2012;57(1), 48-57.

5. **Eltahawy, N., Abd El-Hady, A., Badawi, M., & Hammad, A.** Gamma amino butyric acid ameliorates jejunal oxidative damage in diabetic rats. IJPER 2017;51(4), 588-96.

6. **Ceretta, L. B., Réus, G. Z., Abelaira, H. M., Ribeiro, K. F., Zappellini, G., Felisbino, F. F. et al.** Increased oxidative stress and imbalance in antioxidant enzymes in the brains of alloxan-induced diabetic rats. Exp. Diabetes Res. 2012; 1-8.

7. **Abo Gazia, M. M., & Hassan, N. M.** Effect of glabridin on the structure of ileum and pancreas in diabetic rats: a histological, immunohistochemical and ultrastructural study. Nat. sci 2012;10(3), 78-90.

8. **Mabed, M., & Shahin, M.** Mesenchymal stem cell-based therapy for the treatment of type 1 diabetes mellitus. Curr. Stem Cell Res. Ther. 2012;7(3), 179-90.

9. **Ng, A. X. H., Ton, S. H., & Kadir, K. A.** Low-dose Insulin Treatment Ameliorate Glucose Metabolism in Type 1 Diabetic Rats. *Diabetes Metab J* 2016;7(1): 635-42.

10. **Bhatia, E., & Aggarwal, A.** Insulin therapy for patients with type 1 diabetes. *JAPI* 2007;*55*, 29-34.

11. **Yonamine, C. Y., Pinheiro-Machado, E., Michalani, M. L., Freitas, H. S., Okamoto, M. M., Corrêa-Giannella, M. L. et al.** Resveratrol improves glycemic control in insulin-treated

diabetic rats: participation of the hepatic territory. Nutr. Metab. 2016;13-44.

12. **Rchid, H., Chevassus, H., Nmila, R., Guiral, C., Petit, P., Chokaïri, M., et al.** Nigella sativa seed extracts enhance glucose-induced insulin release from rat-isolated Langerhans islets. Fundam. Clin. Pharmacol. 2004;18(5), 525-9.

13. **Al-Logmani, A., & Zari, T.** Long-term effects of nigella sativa L. oil on some physiological parameters in normal and streptozotocin-induced diabetic rats. Int. J. Diabetes Mellit. 2011;1(03), 46 -53.

14. **Ahmad, S., & Beg, Z. H.** Hypolipidemic and antioxidant activities of thymoquinone and limonene in atherogenic suspension fed rats. Food Chem. 2013;138(2-3), 1116-24.

15. **Bamosa, A. O.** A review on the hypoglycemic effect of nigella sativa and thymoquinone. SJMMS 2015;3(1), 2-7.

16. **Sultan, M. T., Butt, M. S., Karim, R., Zia-Ul-Haq, M., Batool, R., Ahmad, S., et al.** Nigella sativa fixed and essential oil supplementation modulates hyperglycemia and allied complications in streptozotocin-induced diabetes mellitus. Evid.-based Complement. Altern. Med. 2014;2(6), 234-45.

17. **Al-Trad, B., Al-Batayneh, K., El-Metwally, S., Alhazimi, A., Ginawi, I., Alaraj, M. et al.** Nigella sativa oil and thymoquinone ameliorate albuminuria and renal extracellular matrix accumulation in the experimental diabetic rats. Eur Rev Med Pharmacol Sci. 2016;20(12), 2680-8.

18. **El Rabey, H. A., Al-Seeni, M. N., & Bakhashwain, A. S.** The antidiabetic activity of Nigella sativa and propolis on streptozotocin-induced diabetes and diabetic nephropathy in male rats. Evid.-based Complement. Altern. Med. 2017;5439645.

19. **Abdelrazek, H., Kilany, O. E., Muhammad, M. A., Tag, H. M., & Abdelazim, A. M.** Black seed thymoquinone improved insulin secretion, hepatic glycogen storage, and oxidative stress in streptozotocin-induced diabetic male Wistar rats. Oxid. Med. Cell. Longev. 2018; 8104165.

20. **Bouwens, L., Houbracken, I., & Mfopou, J. K.** The use of stem cells for pancreatic regeneration in diabetes mellitus. Nat. Rev. Endocrinol. 2013;9(10), 598-606.

21. **Ayala-Lugo, A., Tavares, A. M., Paz, A. H., Alegretti, A., Miquelito, L., Bock, H. et al.** Age-dependent availability and functionality of bone marrow stem cells in an experimental

model of acute and chronic myocardial infarction. Cell Transplant. 2011**;**20(3), 407-19.

22. **Wang, J., Yu, L., Jiang, C., Chen, M., Ou, C., & Wang, J.** Bone marrow mononuclear cells exert long-term neuroprotection in a rat model of ischemic stroke by promoting arteriogenesis and angiogenesis. BBI - Health 2013*;34*, 56-66.

23. **Castiglione, R. C., Maron-Gutierrez, T., Barbosa, C. M., Ornellas, F. M., Barreira, A. L., Carolina, B. A. et al.** Bone marrow-derived mononuclear cells promote improvement in glomerular function in rats with early diabetic nephropathy. Cell. Physiol. Biochem. 2013;32(3), 699-718.

24. **Usach, V., Malet, M., López, M., Lavalle, L., Piñero, G., Saccoliti, M. et al.** Systemic transplantation of bone marrow mononuclear cells promotes axonal regeneration and analgesia in a model of wallerian degeneration. *Transplantation,* 2017;101(7), 1573-86.

25. **Fontes, E. B., Borges, A. P. B., Pippi, N. L., Rosa, M., Sprada, A. et al.** Overlapping of mononuclear cells derived from bone marrow in rats' intervertebral discs: an in vitro study. CR 2010;40*(4)*, 900-6.

26. **Sen, S., Roy, M., & Chakraborti, A. S.** Ameliorative effects of glycyrrhizin on streptozotocin-induced diabetes in rats. JPP 2011;63(2), 287-96.

27. **Abbasnezhad, A., Hayatdavoudi, P., Niazmand, S., Mahmoudabady, M.** The effects of hydroalcoholic extract of nigella sativa seed on oxidative stress in hippocampus of STZ-induced diabetic rats. AJP 2015;5(4), 333- 40.

28. **Mohamed, S. S., Ali, E. A., & Hosny, S.** The antidiabetic effect of mesenchymal stem cells vs. nigella sativa oil on streptozotocin induced type 1 diabetic rats. J. cell sci. ther. 2015;6(5), 1000226.

29. **El Gawly, H. W., Tawfik, M. K., Rashwan, M. F., Baruzaig, A. S.** The effect of pioglitazone on the liver of streptozotocin-induced diabetic albino wistar rats. Eur Rev Med Pharmacol Sci.2009;13*(6)*, 443-51.

30. **Nabil, A., Hozayen, W. G., Sobh, M., Mahmoud, K., Lotfy, A., El Karef, A. et al.** Effect of antioxidants and mesenchymal stem cells on cisplatin induced renal fibrosis in rats. JSRT 2016;1(4):150-58.

31. **Moir, A. M., & Zammit, V. A.** Effects of insulin treatment of diabetic rats on hepatic partitioning of fatty acids between oxidation and esterification, phospholipid and acylglycerol synthesis, and on the fractional rate of secretion of triacylglycerol in vivo. Biochem. J. 1994;304(1), 177-82.

32. **Elmansy, R. A., & Almasry, S. M.** Morphological and immunohistochemical analysis of the effects of thymoquinone on the neurovascular component of Jejunal submucosa of diabetic rat model. Am. J. Sci. 2013;9(7):224-36.

33. **Atli, O., Ilgin, S., Altuntas, H., & Burukoglu, D.** Evaluation of azithromycin induced cardiotoxicity in rats. Int J Clin Exp Med. 2015;8(3), 3681-90.

34. **Bancroft, J. D., & Gamble, M. (Eds.).** Theory and practice of histological techniques. Elsevier health sciences. 6th edition. Churchill Livingstone, Elsevier, China. **2008.**

35. **Fischer, A. H., Jacobson, K. A., Rose, J., & Zeller, R.** Hematoxylin and eosin staining of tissue and cell sections. CSH Protoc 2008;(5), 4986.

36. **Thompson, S. W., & Hunt, R. D.** Selected histochemical and histopathological methods. *3rd ed*, SPFD 1966;629-33.

37. **Sheehan, D., & Hrapchak, B. ().** Theory and Practice of Histotechnology, ; Columbus. OH-Battelle Memorial Institute. 2nd ed, **1987**;89-117.

38. **De Freitas, P., Natali, M. R. M., Pereira, R. V. F., Neto, M. H. M., & Zanoni, J. N.** Myenteric neurons and intestinal mucosa of diabetic rats after ascorbic acid supplementation.WJG 2008;14(42), 6518–24.

39. **Meyerholz, D. K., & Beck, A. P.** Principles and approaches for reproducible scoring of tissue stains in research. Lab. Investig. 2018;98(7), 844-55.

40. **Hayat, M.A.** Fixation for electron microscopy. *A Cademic Press. New York.* **1981**

41. **Gotfried, J., Priest, S., & Schey, R.** Diabetes and the Small Intestine. Curr. treatm. opt. gastroenterol. 2017;15 (4), 490-507.

42.**Feng X and Li XQ.** The prevalence of small intestinal bacterial overgrowth in diabetes mellitus: a systematic review and meta-analysis. Aging (Albany NY). 2022;14(2):975-88.

43.**Moezi, L., Arshadi, S. S., Motazedian, T., Seradj, S. H., & Dehghani, F.** Anti-diabetic effects of Amygdalus lycioides spach in streptozocin-induced diabetic rats. IJPR 2018;17(1), 353 -64.

44. **Ranjbaran H, Mohammadi Jobani B, Amirfakhrian E, Alizadeh-Navaei R.** Efficacy of mesenchymal stem cell therapy on glucose levels in type 2 diabetes mellitus: A systematic review and meta-analysis. J Diabetes Investig 2021;12(5):803-10.

45. **Hamdan A, Haji Idrus R, Mokhtar MH.** Effects of Nigella Sativa on Type-2 Diabetes Mellitus: A Systematic Review. Int J Environ Res Public Health 2019;5;16(24):4911.

46. **Arikawe, A. P., Oyerinde, A., Olatunji-Bello, I. I., & Obika, L. F. O.** Streptozotocin diabetes and insulin resistance impairment of spermatogenesis in adult rat testis: central Vs local mechanism. Niger J Physiol Sci 2012;27(2), 171-9.

47. **Mahmoodi, M., Koohpeyma, F., Saki, F., & Maleksabet, A.** The protective effect of Zataria multiflora Boiss. hydroalcoholic extract on TNF-α production, oxidative stress, and insulin level in streptozotocin-induced diabetic rats. AJP 2019;9(1), 72 –83.

48. **Niyomchan, A., Sricharoenvej, S., Lanlua, P., & Baimai, S. ().** Cerebellar synaptopathy in streptozotocin-induced diabetic rats. J. Morphol. 2019;37(1), 28-35.

49. **Mohan, Y., Jesuthankaraj, G. N., & Ramasamy Thangavelu, N.** Antidiabetic and antioxidant properties of Triticum aestivum in streptozotocin-induced diabetic rats. Adv Pharmacol Sci 2013; 1-9.

50. **Piccolo, B. D., Graham, J. L., Kang, P., Randolph, C. E., Shankar, K., Yeruva, L. et al.** Progression of diabetes is associated with changes in the ileal transcriptome and ileal-colon morphology in the UC Davis Type 2 Diabetes Mellitus rat. Physiol. Rep. 2021;9, e15102.

51. **Lerkdumnernkit N., Sricharoenvej S., Lanlua P., Niyomchan A., Baimai S., Chookliang A. et al.** The Effects of Early Diabetes on Duodenal Alterations in the Rats. J. Morphol. 2022;40(2), 389-95.

52. **Brenneman, M., Sharma, S., Harting, M., Strong, R., Cox Jr, C. S., Aronowski, J. et al.** Autologous bone marrow mononuclear cells enhance recovery after acute ischemic stroke in young and middle-aged rats. JCBFM 2010;30(1), 140-9.

53. **Ruiz-Salmeron, R., De La Cuesta-Diaz, A., Constantino-Bermejo, M., Pérez-Camacho, I., Marcos-Sánchez, F., Hmadcha, A. et al.** Angiographic demonstration of neoangiogenesis after intra-arterial infusion of autologous bone marrow mononuclear cells in diabetic patients with critical limb

ischemia. Cell Transplant. 2011;20(10), 1629-39.

54. **Xu J. and Zuo C.** The Fate Status of Stem Cells in Diabetes and its Role in the Occurrence of Diabetic Complications. Frontiers in Molecular Biosciences, Sec. Cellular Biochemistry. Front. Mol. Biosci. 2021;8.

55. **Li, X. J., Li, C. Y., Bai, D., and Leng, Y.** Insights into stem cell therapy for diabetic retinopathy: a bibliometric and visual analysis. Neural Regen. Res. 2021;16 (1), 172–8.

56. **Alsuhaibani, A. M.** Effect of nigella sativa against cisplatin induced nephrotoxicity in rats. Ital. J. Food Saf. 2018;7(7242), 105-9.

57. **Farooqui, Z., Afsar, M., Rizwan, S., Khan, A. A., & Khan, F.** Oral administration of nigella sativa oil ameliorates the effect of cisplatin on membrane enzymes, carbohydrate metabolism and oxidative damage in rat liver. Toxicol. Rep. 2016;*3*, 328-35.

58. **Hannan J.M.A., Prawej Ansari, Afra Haque, Afrina Sanju, Abir Huzaifa, Anisur Rahman, et al.** Nigella sativa stimulates insulin secretion from isolated rat islets and inhibits the digestion and absorption of $(CH2O)_n$ in the gut. Biosci Rep 2019;39 (8): BSR20190723.

59. **Alireza Rahmani, Bahram Niknafs, Mohsen Naseri, Maryam Nouri, Ali Tarighat-Esfanjani.** "Effect of Nigella Sativa Oil on Oxidative Stress, Inflammatory, and Glycemic Control Indices in Diabetic Hemodialysis Patients: A Randomized Double-Blind, Controlled Trial", Evid.-based Complement. Altern. Med. **2022;**9. doi:10.1155/2022/2753294

60. **Charlton, M., Ahlman, B., & Nair, K. S.** The effect of insulin on human small intestinal mucosal protein synthesis. Gastroenterol. 2000;118(2), 299-306.

SUPPLEMENTARY
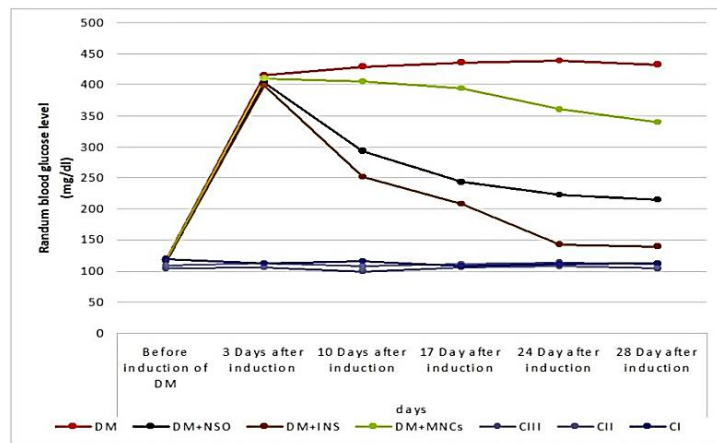
Chart 1: Mean of random blood glucose level in the different studied groups throughout the study
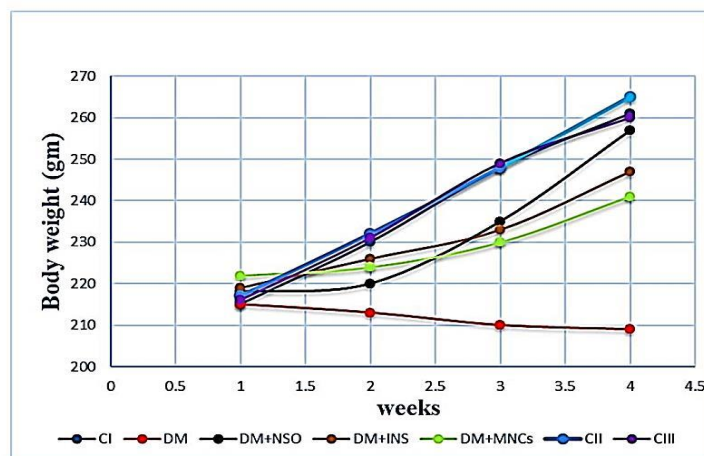
Chart 2: The body weight of different groups throughout the study

Figures (6-22)
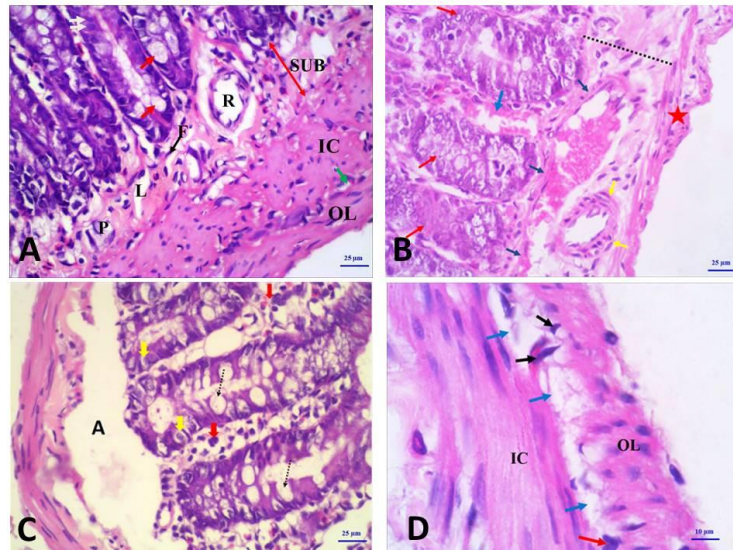
Figure 6: Photomicrographs of sections in rat jejunum of the diabetic group showing:

(A) crypts with lining columnar epithelium (white arrows), distended goblet cells (red arrows), edematous submucosa (SUB) with lymph vessel (L), fibroblasts (F), dilated thick walled submucosal capillary with development of perivascular space (R), thick inner circular (IC) and outer longitudinal muscle layer (OL) with poor organization of muscle fibers and abnormal shaped Meissner's plexus (P) and myenteric plexus (green thick arrow). (**H& E, X400**)

(B) hypertrophied crypts with loss of normal cellular organization (red arrow), hemorrhage (blue arrow), edematous submucosa (dashed line), thick walled blood vessel (yellow arrow) and area of atrophied muscle layer (red star). (**H& E, X400**)

(C) degeneration of submucosa and adjacent inner circular layer of musculosa (A), distended goblet cells (dashed arrows), numerous inflammatory cells of lamina propria (red thick arrow) and entero-endocrine cells (yellow thick arrow). (**H& E, X400**).

(D) areas of neuronal loss (blue arrow), few nerve cells (red arrow) and few enteric glial cells (black arrows) in the myenteric ganglia between the inner circular (IC) and outer longitudinal (OL) layers of the musculosa. (**H&E X1000**)
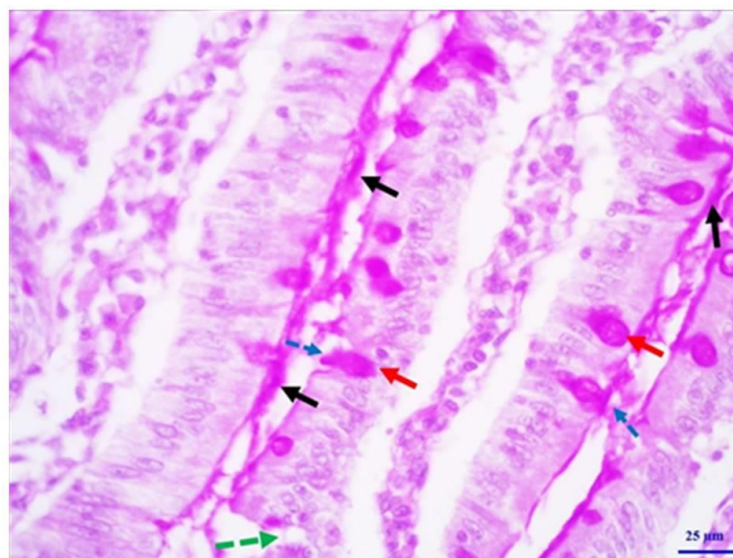
Figure 7: A photomicrograph of a section in rat jejunum of the diabetic group showing jejunal villi with dense thickened positive PAS reaction in villous brush border (black arrows) and numerous goblet cells over-distended with dense positively PAS -stained material (red arrows) pouring its contents to the surface (dashed blue arrow) with areas of epithelial discontinuation (dashed green arrow). (**PAS, X400**)
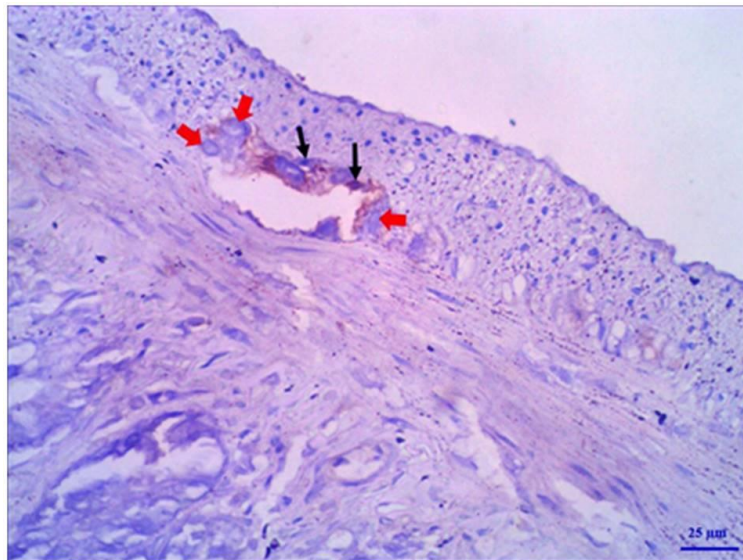
Figure 8: A photomicrograph of a section in jejunum in diabetic group showing small-sized myenteric plexus formed of few numbers of GFAP-positive immune-stained enteric glial cells with less prominent processes (black arrows) and negatively immune-stained nerve cells (red thick arrows). **(GFAP-immunostain, X 400)**
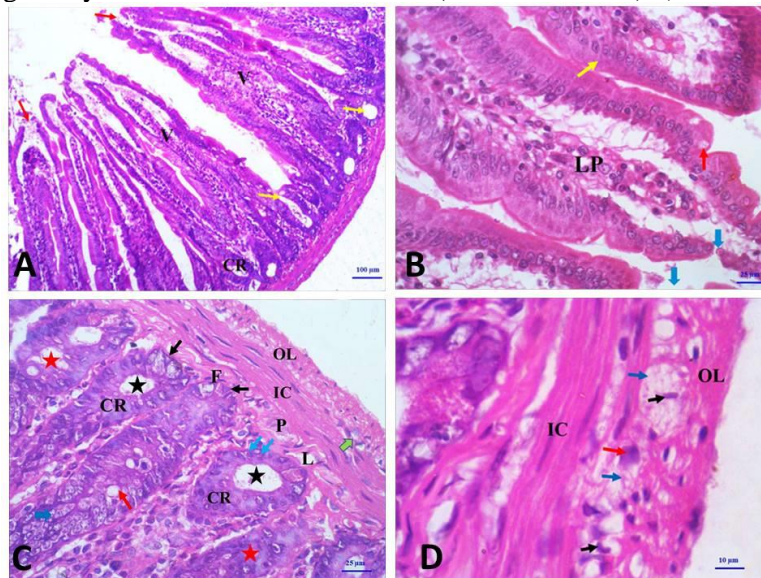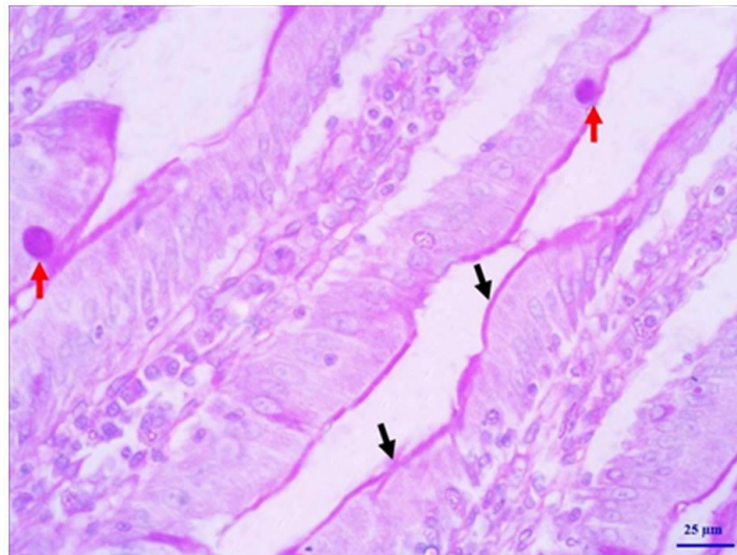

Figure 9: Photomicrographs of sections in rat jejunum of the DM+MNCs group showing:
- **(A)** hypertrophied fused villi (V) with villous surface epithelium shedding (red arrow), intact crypts (CR) with cystic dilatation of some other crypts (yellow arrows). **(H&E, X100)**
- **(B)** villi formed of lamina propria (LP) covered by a single layer of tall columnar cells with oval basal nuclei (yellow arrow), few goblet cells (red arrow) and areas of surface epithelium loss (blue arrows). **(H&E, X 400)**
- **(C)** distortion of some crypt (red stars), other crypts are intact (CR) with cystic dilatation of its lumen (black stars). Crypts lined with columnar epithelium (blue arrow), paneth cells (black arrow), and goblet cells (red thick arrow). Notice also intact submucosa with lymph vessel (L), fibroblast (F), Meissner's plexus (P), myenteric plexus (green thick arrow) and restoration of the normal organization of inner circular (IC), outer longitudinal muscle layer (OL). **(H&E, X 400)**
- **(D)** mild increased number of nerve cells (red arrow), enteric glial cells (black arrows) and network of unmyelinated nerve fibers (blue arrows) in the myenteric ganglia between the inner circular (IC) and outer longitudinal (OL) layers of the musculosa. **(H&E, X1000)**

Figure 10: A photomicrograph of a section in rat jejunum of the DM+MNCs group showing jejunal villi with moderate intensity and thickness of PAS-positively stained villous brush border (black arrows) and goblet cells filled with PAS stained material (red arrows). (**PAS, X 400**)
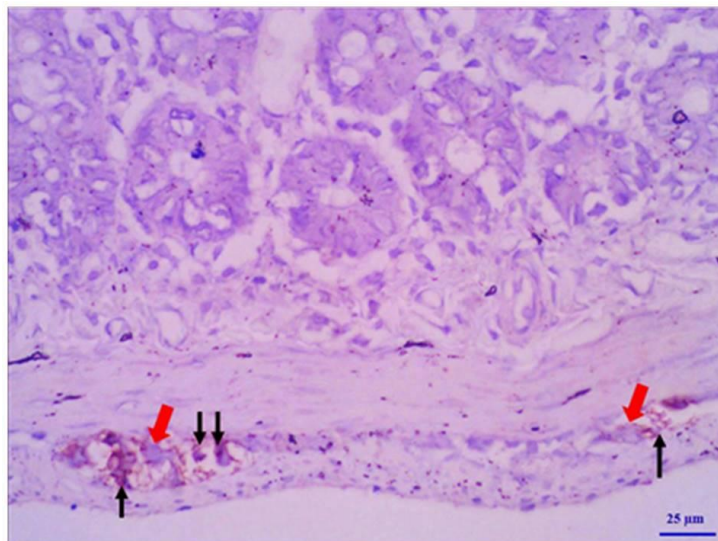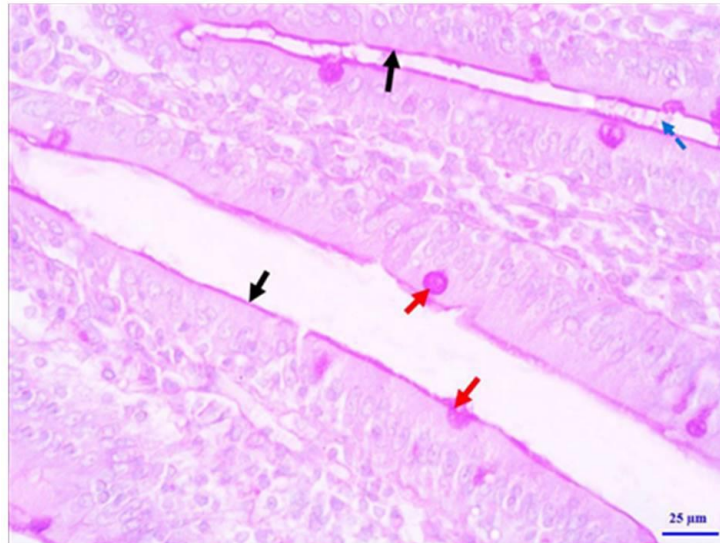

Figure 11: A photomicrograph of a section in rat jejunum of the DM+MNCs group showing myenteric plexus with few numbers of positive GFAP-immune stained enteric glial cells with less prominent processes (black arrows) and nerve cells (red thick arrow). (**GFAP-immunostain, X400**)
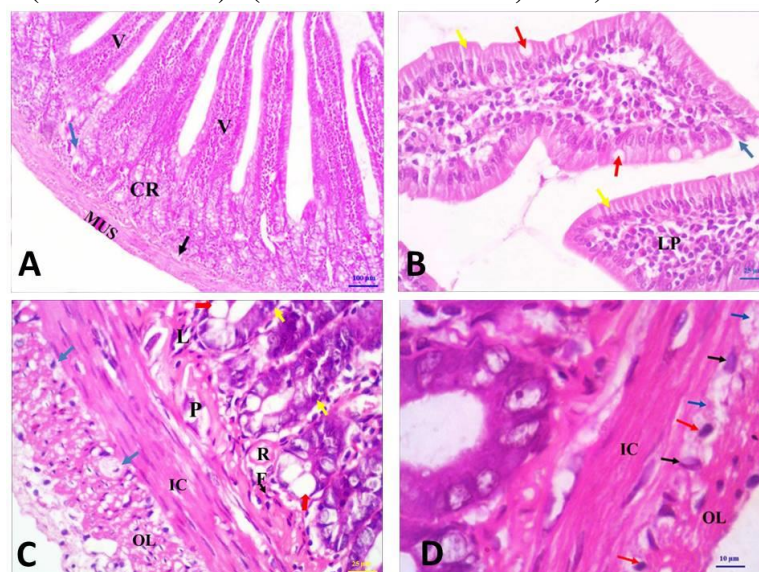
Figure 12: Photomicrographs of sections in rat jejunum of the DM+NSO group showing:

(A) normal architecture of the jejunum, intact villi (V), intact crypts (CR) with area of crypt distortion (blue arrow), intact submucosa (black arrow) and musculosa (MUS) layers. **(H&E, X100)**

(B) normal villous architecture with intact epithelial columnar cells covering (yellow arrows) and scattered goblet cells (red arrows). Notice few inflammatory cells infiltration in lamina propria (LP) and small area of epithelium discontinuity (blue arrow). **(H&E, X400).**

(C) crypts with intact lining columnar epithelium (yellow arrows) and goblet cells (red thick arrows). Intact submucosa lymph vessel (L), fibroblast (F), Meissner's plexus (P), submucosal capillary with normal diameter and wall (R), well organized inner circular (IC) and outer longitudinal muscle layer (OL) with intact myenteric plexus (blue arrows). **(H&E, X400)**

(D) increased number of small sized enteric glial cells (red arrows), nerve cells with large cell bodies (black arrows) and network of unmyelinated nerve fibers (blue arrows) in the myenteric ganglia between the inner circular (IC) and outer longitudinal (OL) layers of the musculosa. **(H&E, X1000)**

Figure 13: A photomicrograph of section of rat Jejunal villi from the DM+NSO group showing mild intensely stained villous brush border (black arrows) and many appropriate-sized goblet cells filled with PAS stained material (red arrows) with few cells pouring its contents to the surface (dashed blue arrow). **(PAS, X400)**
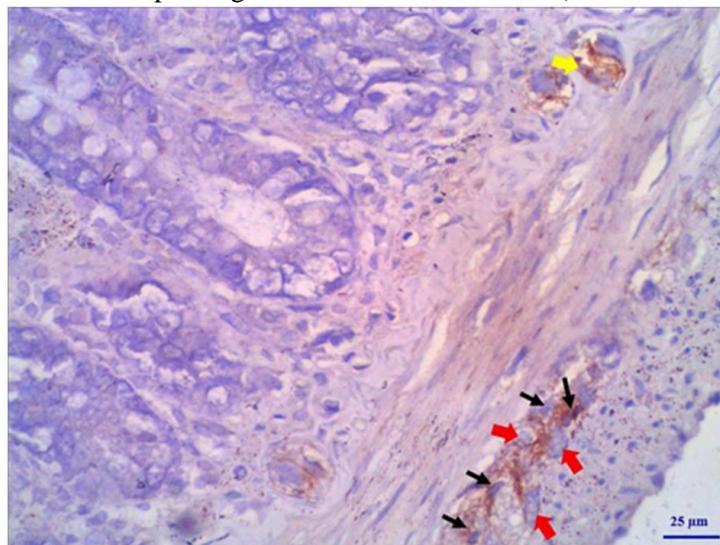

Figure 14: A photomicrograph of a section in rat jejunum of the DM+NSO group showing a myenteric plexus with remarkable increase in GFAP positive immune-expression in enteric glial cells (black arrows) and numerous negative immune reactions in nerve cells (red thick arrow) with positive stained enteric glial cells in the submucosal plexus (yellow thick arrow). **(GFAP-immunostain, X 400)**
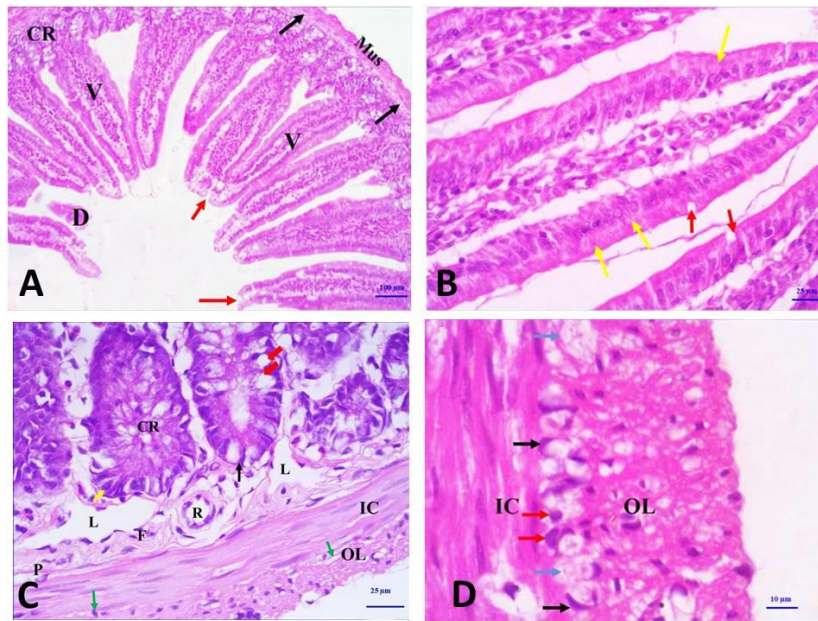
Figure 15: Photomicrographs of sections in rat jejunum of the DM+INS group showing:

(A) normal jejunal architecture, intact villi (V), crypts (CR), submucosa (black arrows) and musculosa (Mus). Note, small areas of sloughing necrotic epithelium into the intestinal lumen (D) and small area of surface epithelium discontinuity (red arrows). **(H&E, X100)**

(B) normal villous architecture, covered by a single layer of tall columnar cells with oval basal nuclei (yellow arrows) with few scattered average sized goblet cells (red arrows). **(H&E, X 400).**

(C) well organized crypts (CR) with intact lining columnar epithelium (yellow arrows), paneth cells (black arrows), and goblet cells (red arrows), dilated submucosal lymph vessel (L), fibroblasts (F), nerve plexus (P), average capillary wall thickness (R), normal architecture of inner circular (IC) and outer longitudinal muscle layers (OL) with scattered myenteric plexus (green arrows). **(H&E, X 400).**

(D) intact nerve cells (red arrows), enteric glial cells (black arrows) and network of unmyelinated nerve fibers (blue arrows) in the myenteric ganglia between the inner circular (IC) and outer longitudinal (OL) layers of the musculosa. **(H&E, X1000)**
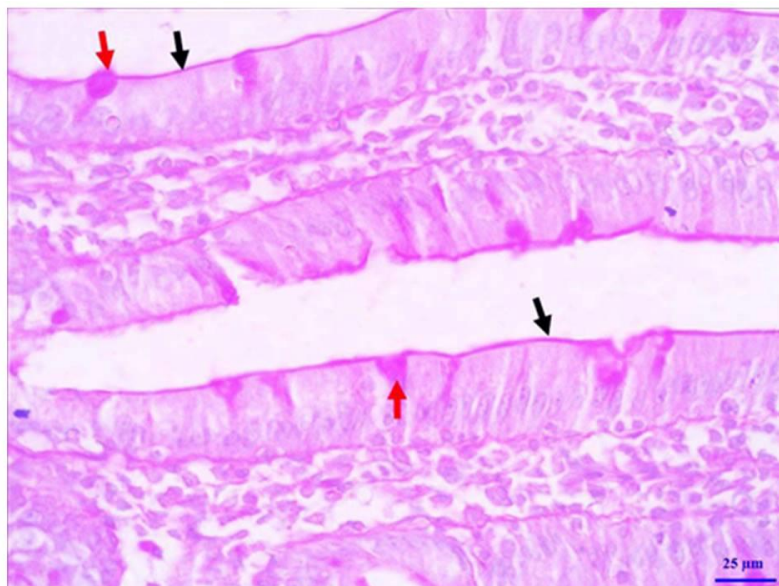

Figure 16: A photomicrograph of a section in rat jejunum in the DM+INS showing jejunal villi with positively stained villous brush border (black arrows) and many appropriate-sized goblet cells filled with positively PAS-stained material (red arrows). **(PAS, X400)**
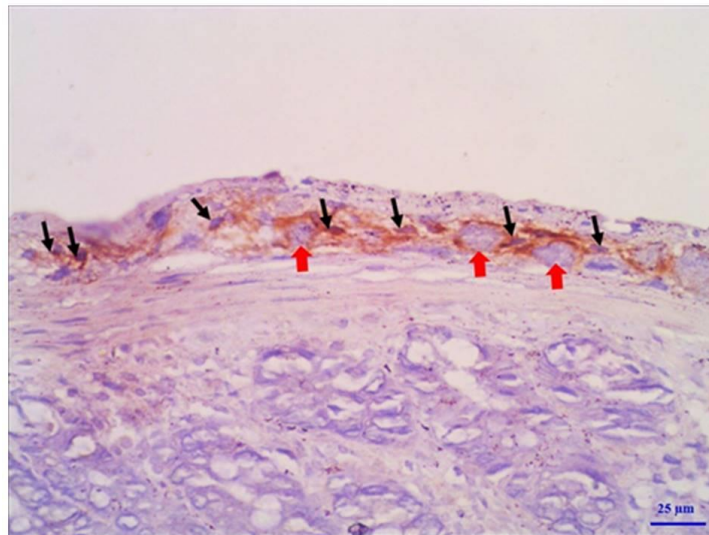
Figure 17: A photomicrograph of a section in rat jejunum of the DM+INS group showing myenteric plexus with remarkable increase in the number of GFAP positive enteric glial cells with prominent process (black arrows) and numerous negatively GFAP immune-stained nerve cells (red thick arrow). **(GFAP-immunostain, X 400)**
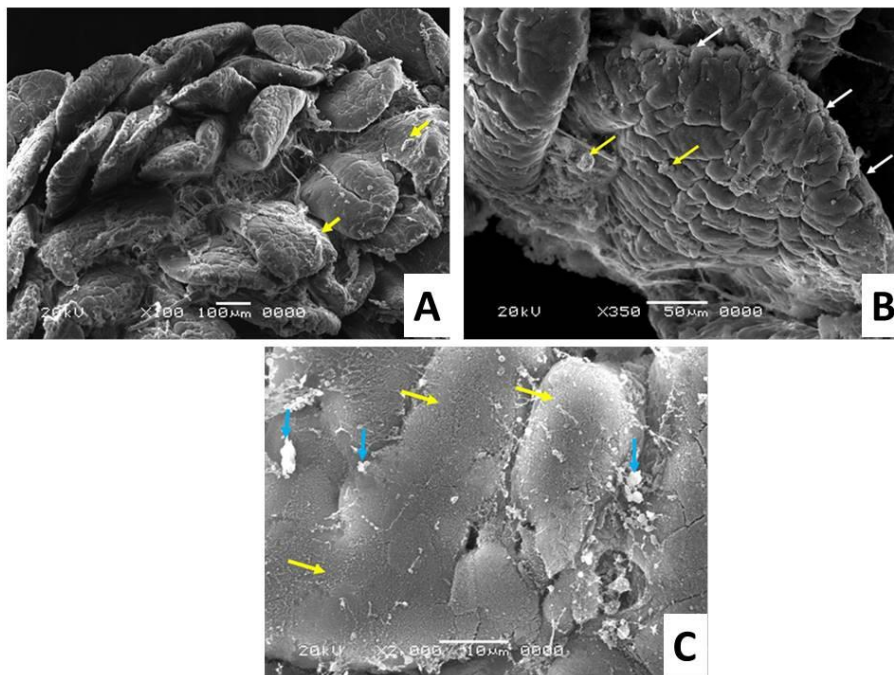

Figure 18: Scanning electron photomicrographs of jejunal villi of the control group showing:
   (A) hexagonal appearance of the villi with intact surface columnar epithelium covered with mucous (yellow arrows). **(X100)**
   (B) intact villous tips (white arrows) with velvet hexagonal appearance and generally smooth surface and pock marks corresponding to the mouths of goblet cells with scattered mucous (yellow arrows) discharged by goblet cells. **(X 350)**
   (C) showing the appearance of a rough surface due to the microvilli of columnar epithelial cells (yellow arrows) and projecting plugs of mucus from goblet cells (blue arrows). **(X 2000)**
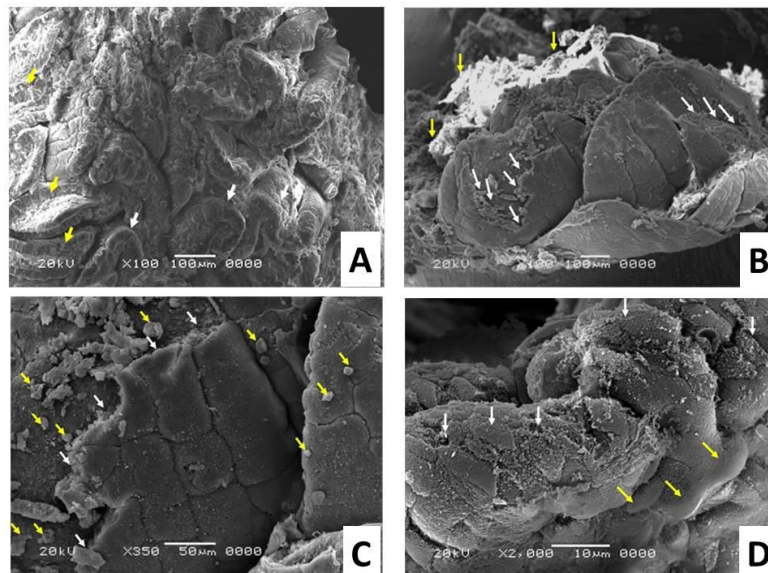
Figure 19: Scanning electron photomicrographs of jejunal villi of the diabetic group showing:
- (A) convoluted broad thick villi with flattened mucosa (white arrows), denudation of the villous epithelial lining of the tips with exposure of the basal lamina (yellow arrows). **(X 100)**
- **(B)** broad villi with multiple sites of necrotic villi with exfoliated epithelium (white arrows) and large mucous plug (yellow arrows). **(X 100)**
- (C) denudation of the epithelial lining of the jejunal villi with exposure of the basal lamina (white arrows) and hyperplasia of goblet cells (yellow arrows). **(X350)**
- (D) areas of exfoliation of the villous epithelial lining (white arrows) and areas of smooth surface with loss of microvilli (yellow arrows). **(X 2000**
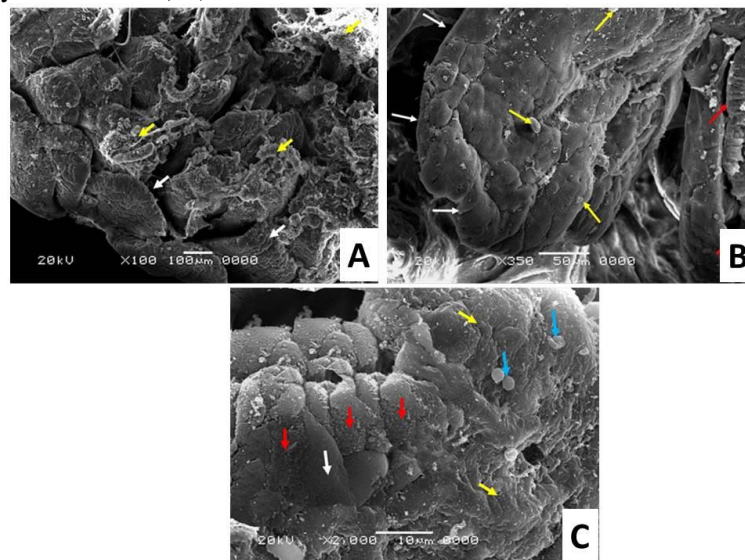

Figure 20: Scanning electron photomicrographs of jejunl villi of the DM-MNCs showing:
- (A) intact villous tips with velvet hexagonal appearance (white arrow) and goblet cells openings covered with mucous (yellow arrows). **(X100)**
- (B) intact villous tips (white arrows) with normal hexagonal appearance and mucous discharged by goblet cells (yellow arrows). Note, a villous with sloughing of epithelial covering of the tips (red arrows). **(X350)**
- (C) normal villous surface (yellow arrows) with mucous discharged of goblet cells (blue arrows), smooth surface with loss of microvilli (white arrow) and areas of epithelial denudation (red arrows). **(X2000)**
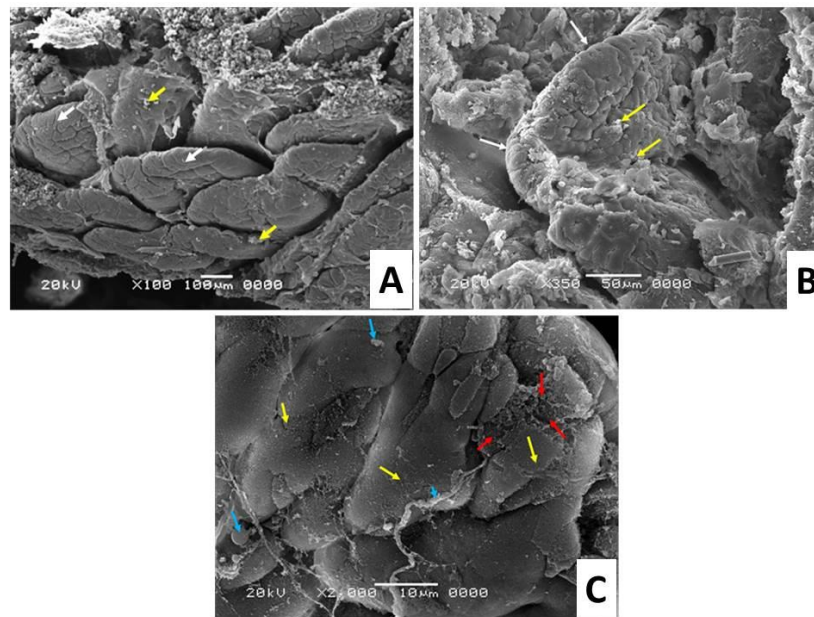
Figure 21: Scanning electron photomicrographs of jejunl villi of the DM+NSO showing:
  (A) intact villous tips with velvet hexagonal appearance (white arrows) and goblet cells openings covered with mucous secretion (yellow arrows). **(X100)**
  (B) intact villous tips (white arrows) and appearance of goblet cells mucous drops (yellow arrows). **(X350)**
  (C) normal appearance of villi surface (yellow arrows), mucus droplets from goblet cells (blue arrows) and small area of exfoliation of the villous epithelial lining (red arrows). **(X 2000)**
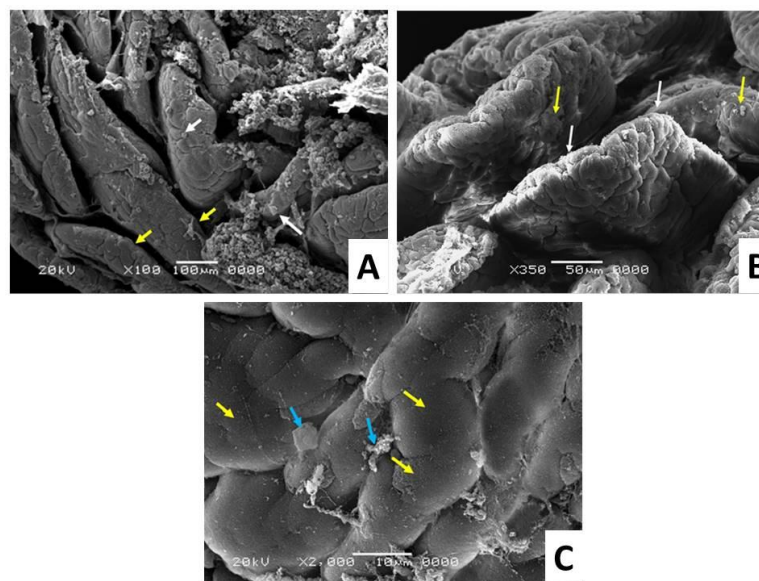

Figure 22: Scanning electron photomicrographs of jejunl villi of the DM+INS showing:
  (A) intact villous tips with velvet hexagonal appearance (white arrows) and appearance of mucous secretion of goblet cells (yellow arrows). **(X100)**
  (B) intact villous tips (white arrows) with normal hexagonal appearance and mucous discharged by goblet cells (yellow arrows). **(X 350)**
  (C) normal appearance of villous surface induced by micro villi (yellow arrows) and mucus droplets from goblet cells (blue arrows). (**X2000**).